

## Scanning-tunneling-microscopy investigation of the Ni(100)- $p(2 \times 2)$ C surface

G. Hörmandinger and J. B. Pendry

*Department of Physics, Imperial College, London SW7 2BZ, United Kingdom*

F. M. Leibsle, P. W. Murray, R. W. Joyner,\* and G. Thornton†

*Interdisciplinary Research Center for Surface Science, University of Liverpool,  
P.O. Box 147, L69 3BX, United Kingdom*

(Received 29 March 1993; revised manuscript received 3 June 1993)

The scanning-tunneling-microscopy (STM) image of the Ni(100)- $p(2 \times 2)$ C surface has been investigated both experimentally and theoretically. The well-known  $p4g$  reconstruction of this surface could not be observed in the STM. Atomic resolution could be achieved only for positive or very small negative sample bias voltage, and even then the Ni atoms were not visible. Surprisingly, for a metallic surface, the corrugation could be observed for a bias voltage of up to +2 V. These observations are explained theoretically by the presence of a surface band gap above the Fermi energy, which causes the tip to come closer for positive voltage than for negative voltage. A model calculation reproduces most of the observations: the absence of the  $p4g$  reconstruction in the image, the asymmetry in the  $I(V)$  spectrum, and the fact that the corrugation is small, are only present at positive voltage and observable up to large voltage. However, the calculated STM image shows the C atoms as depressions while in the experiment, a small protrusion is observed. A more elaborate investigation would be necessary to resolve this discrepancy.

### I. INTRODUCTION

The behavior of carbon adsorbed on the Ni(100) surface has been the subject of extensive research in recent years, motivated by its importance as a catalyst.<sup>1-8</sup> In this paper we look at the carbidic surface phase which is the one involved in the methanation reaction of CO (the Fischer-Tropsch synthesis). The catalytic activity of a metal surface and the influence of adsorbates on it (poisoning) have been discussed in terms of the local density of states (LDOS) at the Fermi energy.<sup>4,9</sup> The scanning tunneling microscope (STM) is a device which is sensitive to this quantity, and in a simplified theory even maps contours of constant LDOS.<sup>10</sup> It is therefore of obvious interest to investigate the behavior of the C/Ni(100) surface in the STM.

A variety of experiments has been performed to establish the geometry of this system.<sup>11-14</sup> The C atoms are sitting in hollow sites deep inside the surface, so that they are nearly coplanar with the top Ni layer [ $d_{\perp} = 0.12$  Å (Ref. 14)]. The four Ni atoms surrounding each carbon are rotated clockwise or counterclockwise, giving rise to a symmetry which contains two perpendicular glide planes (Fig. 1). The corresponding space group is  $p4g$ . This peculiar arrangement shows up in low-energy electron diffraction (LEED) measurements through the absence of certain fractional-order beams at normal incidence. The STM, however, gives information in real space so one might hope to see the Ni atoms in their rotated positions. The STM does not, however, image the positions of the atomic cores, rather it detects variations in the local electronic structure. For example, one can

distinguish between the faulted and unfaulted halves of the Si(111)- $(7 \times 7)$  unit cell with the sample biased negatively but not with the sample biased positively. Height variations measured by STM (Ref. 15) between the two halves of the unit cell are also greater than those determined by helium scattering.<sup>16</sup> Oxygen, even though it is adsorbed above the surface of Ni(100), appears as a

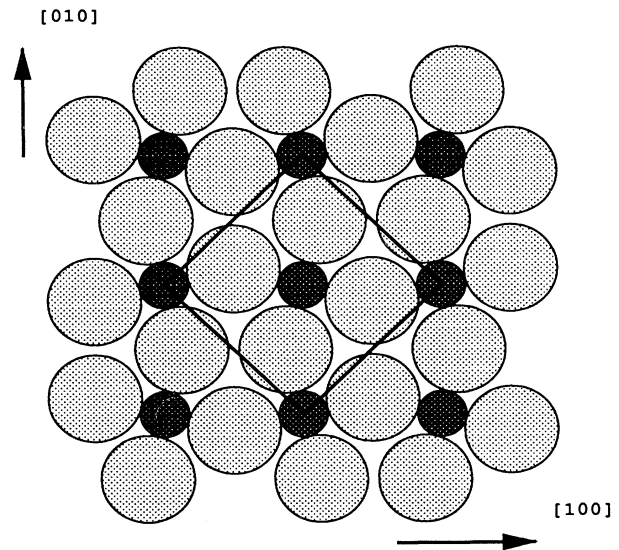


FIG. 1. A symbolic view of the  $p4g$  reconstruction of Ni(100)- $p(2 \times 2)$ C.

depression because of its influence on the local density of electronic states.<sup>17</sup> Interpretations of STM images can be somewhat speculative, and indeed in many cases authors often refrain from making elemental assignments of features within their STM images, hence interpretations of STM images with atomic resolution should be viewed with caution and ideally be combined with a theoretical analysis.

## II. EXPERIMENT

These results were obtained using a commercial Omicron Vakuumphysik STM operated in a conventional ultrahigh vacuum (UHV) chamber with a base pressure of  $\leq 10^{-10}$  mbar. The chamber was also equipped with facilities for ion argon bombardment, a quadrupole mass spectrometer for monitoring gas purities, and a four-grid rear view LEED/Auger retarding field analyzer for checking sample order and cleanliness prior to imaging with the STM.

The Ni(100) sample was mounted on a Ta sample holder by Ta clips and was washed in methanol before being inserted into the vacuum chamber via a fast entry lock. The sample was thoroughly outgassed and cleaned *in situ* by repeated cycles of argon ion bombardment and annealing to 920 K until a sharp  $1 \times 1$  LEED pattern and clean Auger spectra were observed. Sample heating was obtained by using electron beam bombardment with electrons striking the back of the baseplate, while temperatures were monitored using a Chromel-Alumel thermocouple mounted on the manipulator approximately 2 cm from the sample.

Carbon was deposited onto the sample by exposing the clean surface to a pressure of  $1 \times 10^{-7}$  mbar of  $C_2H_4$  for 10 min while maintaining the sample temperature at 520 K. This then produced a  $(2 \times 2)p4g$  LEED pattern. When the sample temperature had dropped to near room temperature, it was removed from the manipulator via a wobble stick and placed in the STM.

Imaging was carried out in the constant current and spectroscopy modes. With this STM the tip is maintained at ground potential while the sample is biased. Constant current topographs were obtained for a variety of sample bias and tunneling currents to find a set of parameters that optimized atomic resolution for this surface. Typically, when trying to obtain atomic resolution images, we took  $80 \times 80$  Å scans with 0.3–0.5 Å pixel increments. Spectroscopy data were recorded by taking constant current topographs and measuring the  $I$ - $V$  characteristics for each pixel point of the image by temporarily breaking the feedback loop and ramping the voltage between the sample and tip over a predetermined range. In general, we chose to simultaneously acquire two constant current topographs and two sets of  $I$ - $V$  characteristics. The software that controls the STM allows us to make a line scan over the sample with one set of feedback conditions, stopping at each pixel to take an  $I(V)$  curve and then go back over the same line with another set of feedback conditions, also stopping at each pixel to take an  $I(V)$  curve. This was an attempt to keep all factors such as tip changes and thermal drift to a minimum

in order to increase the likelihood that the spectroscopy curves would reflect the electronic structure of the sample. In order to average over a large number of unit cells, we typically took scans over  $80 \times 80$  Å areas with 1 Å increments; the voltages were ramped between  $-2$  V and  $+2$  V with 0.2 V increments. Each pair of spectroscopy images required approximately 1 Mbyte of data storage.

## Experimental results

In general it was somewhat difficult to obtain atomic resolution images of this surface. We found that the corrugations observed were rather faint and on the order of 0.02 Å. Figure 2 shows a  $20 \times 20$  Å constant current topograph of the Ni(100)- $(2 \times 2)$ -C( $p4g$ ) surface taken at  $-0.007$  V, 1.0 nA. This image shows atomic scale corrugations appearing in a square-shaped array of protrusions covering the surface. The dimensions and orientation of these square arrays are consistent with a  $c(2 \times 2)$  unit cell which suggests, according to the model shown in Fig. 1, that the observed corrugations are associated with the positions of the carbon atoms rather than the nickel. In Fig. 2, a  $c(2 \times 2)$  unit cell is outlined. Features on this image were typical of those taken at different locations on the surface. The reconstruction was observed to extend fairly uniformly across terraces with occasionally irregularly shaped antiphase domain boundaries. Steps did not appear to be stabilized in any particular direction by the reconstruction.

As mentioned earlier, atomic resolution images revealed a square array of protrusions with spacing and orientations consistent with a  $c(2 \times 2)$  unit cell. Since the carbon atoms are arranged in a  $c(2 \times 2)$  pattern with respect to the substrate, it is easy to conclude that the corrugations observed are associated with the carbon atoms, a more difficult question is whether the carbon atoms ap-

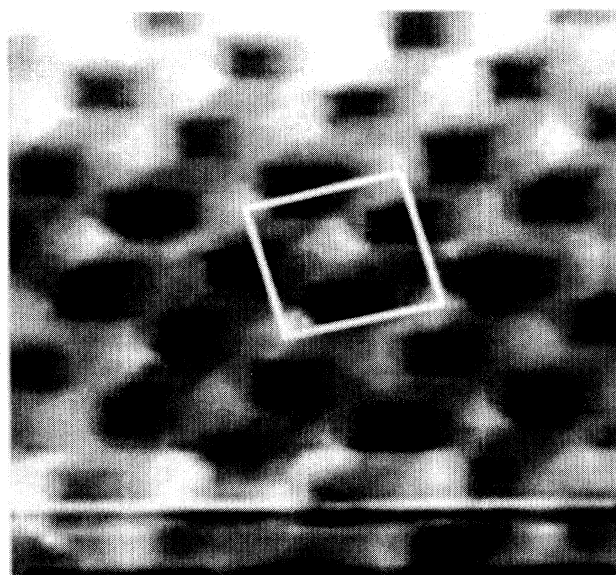


FIG. 2. A  $20 \text{ Å} \times 20 \text{ Å}$  image of the Ni(100)- $(2 \times 2)$ C  $p4g$  surface taken at  $-0.007$  V, 1.0 nA with the  $c(2 \times 2)$  unit cell outlined.

TABLE I. Experimental corrugation heights at various tunneling conditions.

Bias voltage (V)	Tunneling current (nA)		Corrugation height (Å)
	$\pm 0.001$	$\pm 0.1$	
-0.020		1.0	0.07
-0.007		1.0	0.03
-0.006		1.0	0.02
-0.004		1.0	0.03
-0.002		2.0	0.05
0.010		0.5	0.07
0.050		1.0	0.04
0.100		1.0	0.03

pear as protrusions or depressions. Oxygen on Ni(100) adsorbs in fourfold hollow sites and appears as a depression on the surface,<sup>17</sup> while sulfur also adsorbs in fourfold hollow sites but appears as a protrusion.<sup>18</sup> Both result in very similar images. It was concluded on the basis of coverage dependent images that oxygen appeared as a depression, while it was concluded on the basis of the appearance of the atoms around defects and codomains of the  $c(2 \times 2)$  S reconstruction that S appears as a protrusion. We observed that the most common defect in our atomic resolution images was the occasional absence of a protrusion. This defect can be easily explained by the assumption that the carbon atoms appear as protrusions and that the defect is caused by a missing carbon atom. It is very difficult to assume that the carbon atoms appear as depression and then devise a credible explanation for such a defect.

Figure 3 shows a typical height profile taken along the [100] direction and Table I contains measured corrugation heights for a number of both negative and positive bias conditions. In general, we found that we could obtain atomic resolution for only very low voltages. However, while we were acquiring constant current topographs during the taking of spectroscopy data, we observed 0.03 Å corrugations occurring with a sample bias of 1.0 V and a tunneling current of 1 nA. No such corrugation was ob-

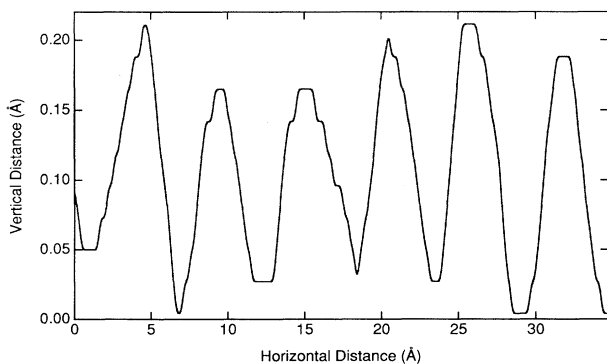


FIG. 3. A height profile taken along the [100] direction of the Ni(100)-(2×2)C  $p4g$  surface using scanning parameters of  $-0.01$  V, 0.5 nA.

TABLE II. The experimental tunneling current  $I$  at  $\pm 2$  V for various feedback conditions. The average of the ratio  $I(+2 \text{ V})/I(-2 \text{ V})$  is  $-0.71$ .

Feedback conditions		Tunneling current at	
Voltage (V)	Current (nA)	$-2$ V	$+2$ V
-3.5	1.0	-0.02	0.02
-3.0	1.0	-0.30	0.31
-2.5	1.0	-0.56	0.44
-2.0	1.0	-0.94	0.62
-1.5	1.0	-1.31	0.85
-1.0	1.0	-1.97	1.32
-0.5	1.0	-6.04	4.26
+0.5	1.0	-10.89	7.28
+1.0	1.0	-4.69	2.97
+1.5	1.0	-2.15	1.75
+2.0	1.0	-1.64	0.94
+2.5	1.0	-0.93	0.63
+3.0	1.0	-0.41	0.38
+3.5	1.0	-0.47	0.09

served in the simultaneously acquired image taken with  $-1.0$  V sample bias.

Figure 4 shows a pair of spectroscopy curves formed by averaging over the entire  $80 \times 80$  Å image obtained simultaneously with feedback conditions  $\pm 2$  V, 1 nA. For the spectroscopy curve obtained with tunneling conditions of 2 V and 1 nA, the feedback loop forces the tunneling current at  $+2$  V to be 1 nA, however, at  $-2$  V the magnitude of the tunneling current at is  $>1.5$  nA. At feedback conditions of  $-2.0$  V and 1 nA, the current detected at  $+2.0$  V during the acquisition of spectroscopy data is only 0.62. This trend was quite reproducible for spectroscopic images taken under feedback conditions 1 nA tunneling currents and bias voltages of  $\pm 0.5$ ,  $\pm 1.0$ ,

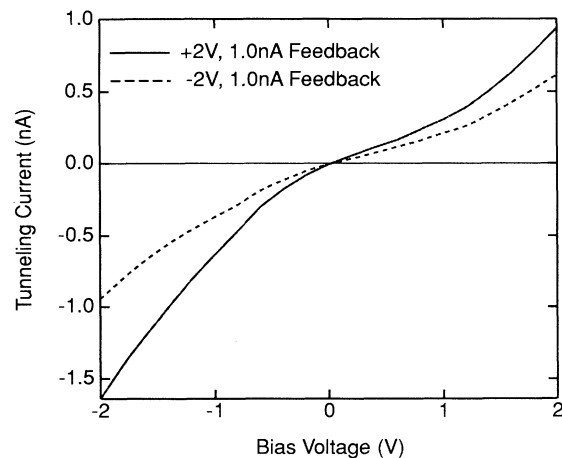


FIG. 4. Spectroscopy curves averaged over an  $80 \text{ Å} \times 80 \text{ Å}$  area of the Ni(100)-(2×2)C  $p4g$  surface taken with feedback conditions of  $-2$  V, 1.0 nA (dashed line) and  $+2$  V, 1.0 nA (solid line) with the voltage being ramped in increments of 0.2 V from  $+2$  V to  $-2$  V.

$\pm 1.5$ ,  $\pm 2.0$ ,  $\pm 2.5$ , and  $\pm 3.0$  V. If we assume a symmetric density of states about the Fermi level for the tip then these asymmetries in the endpoints of the spectroscopy curves can be explained by the density of states of the sample above the Fermi level being less than those below. The values of the tunneling currents at the endpoints of the voltage ramp are shown in Table II.

### III. THEORY

#### A. General principles

Following the ideas of Tersoff<sup>19</sup> and Tersoff and Hamann,<sup>10</sup> the STM image of a surface can be linked to its electronic structure by looking at the  $z$  dependence of wave functions at different points in reciprocal space. Assuming a step barrier of height  $V$ , then a wave of energy  $E$  and a wave vector  $\mathbf{k}_{||}$  parallel to the barrier will decay inside the barrier as  $\exp(-\kappa z)$ , with  $z$  pointing into the barrier, and with the decay constant

$$\kappa = \sqrt{k_{||}^2 + 2(V - E)} \quad (1)$$

(where atomic Hartree units  $e = \hbar = m_e = 1$  are used). Consequently, waves with small  $\mathbf{k}_{||}$  will reach out farthest into the vacuum. In the framework of the transfer Hamiltonian, or Bardeen's approximation, the tunneling current is given by a sum over tunneling matrix elements  $M_{\mu\nu}$  linking states  $\psi_\mu$  of one system (the tip, say) with

states  $\psi_\nu$  of the other system (the sample):

$$I = 2\pi \sum_{\mu,\nu} |M_{\mu\nu}|^2 \delta(E_\mu - E_\nu), \quad (2)$$

$$M_{\mu\nu} = \frac{1}{2} \int d\mathbf{S} (\psi_\mu^* \nabla \psi_\nu - \psi_\nu \nabla \psi_\mu^*). \quad (3)$$

The double sum in Eq. (2) extends over states within the allowed energy range, defined by the applied bias voltage  $V_B$ . The surface integral in Eq. (3) is over an interface between tip and sample. Assuming a periodic structure for the sample surface, the sample states  $\psi_\nu$  are Bloch functions labeled  $\mathbf{k}_{||}$  which can be expressed as a sum over the two-dimensional reciprocal lattice. Inside the barrier,  $\psi_\nu$  is of the form

$$\psi_\nu = \sum_g a_g \exp \left[ (\mathbf{k}_{||} + \mathbf{g}) \mathbf{r}_{||} - \sqrt{(\mathbf{k}_{||} + \mathbf{g})^2 + 2(V - E)} z \right]. \quad (4)$$

The squared matrix element in Eq. (2) thus leads to a double sum over two-dimensional reciprocal lattice vectors  $\mathbf{g}, \mathbf{g}'$ . The sum over sample states implies a  $\mathbf{k}_{||}$  integral over the surface Brillouin zone (BZ). By slightly rearranging the lattice sums, we can write the tunneling current in the form

$$I(V_B, \mathbf{r}) = \sum_{\mathbf{G}} e^{i\mathbf{G} \cdot \mathbf{r}_{||}} \int_0^{V_B} dE \int_{\text{BZ}} d^2 k_{||} \sum_g f(\mathbf{k}_{||}, \mathbf{G}, \mathbf{g}) \sigma(E, \mathbf{k}_{||}, \mathbf{G}, \mathbf{g}). \quad (5)$$

Here we have put all the band structure information about the sample and the tip into the factor  $\sigma(E, \mathbf{k}_{||}, \mathbf{G}, \mathbf{g})$ . The tip height  $z$ , however, is exclusively contained in the factor  $f(\mathbf{k}_{||}, \mathbf{G}, \mathbf{g})$  which just contains the exponential tails of the wave functions:

$$f(\mathbf{k}_{||}, \mathbf{G}, \mathbf{g}) = \exp \left[ -\sqrt{(\mathbf{k}_{||} + \mathbf{g} + \mathbf{G})^2 + 2(V - E)} z - \sqrt{(\mathbf{k}_{||} + \mathbf{g})^2 + 2(V - E)} z \right]. \quad (6)$$

To avoid confusion, we have left the energy and  $z$  dependence of the factor  $f(\mathbf{k}_{||}, \mathbf{G}, \mathbf{g})$  implicit. The larger  $|\mathbf{G}|$ , the stronger  $f(\mathbf{k}_{||}, \mathbf{G}, \mathbf{g})$  decays as a function of  $z$ , which causes the STM image to be smooth, in general, with only a cosinelike spatial variation. Viewed as a function of  $\mathbf{k}_{||}$ ,  $f(\mathbf{k}_{||}, \mathbf{G}, \mathbf{g})$  has a single peak at the position  $\mathbf{k}_{||} = \mathbf{g} - \mathbf{G}/2$ , that is, midway between two reciprocal lattice points which are separated by  $\mathbf{G}$ . That is, it acts as a weighting function, selecting different regions in  $K$  space for different terms in the STM current. Away from this peak, the factor rapidly drops to zero. This behavior has immediate consequences for the STM image.

Consider first the zero-order term ( $\mathbf{G} = \mathbf{0}$ ) which de-

scribes the  $\mathbf{r}_{||}$ -independent part of the current. It is by far the most prominent one and its  $z$  dependence determines the average tip distance for a given current. The factor  $f(\mathbf{k}_{||}, \mathbf{G} = \mathbf{0}, \mathbf{g})$  is peaked at the reciprocal lattice point  $\mathbf{k}_{||} = \mathbf{g}$  [see Fig. 5(a)], and since we are integrating only over the first Brillouin zone, the peak at the  $\bar{\Gamma}$  point is the most important one. If there are many sample states available at the  $\bar{\Gamma}$  point and at the energy in question, then the current will be large or, in constant current mode, the tip will stay comparatively far away from the sample. If, on the other hand, there is a band gap around  $\bar{\Gamma}$ , then the tip will have to come closer.

The corrugation will, in general, be determined by the smallest nonzero lattice vector  $\mathbf{G}$ . The corresponding factor  $f(\mathbf{k}_{||}, \mathbf{G}, \mathbf{g})$  has its most important peaks at  $\mathbf{k}_{||} = \pm \mathbf{G}/2$ , i.e., at the Brillouin zone boundary [see Fig. 5(b)]. If the band structure of the sample has states there, then the STM image is likely to be corrugated in the form  $\cos(\mathbf{G} \mathbf{r}_{||})$ . An energy gap at this  $\mathbf{k}_{||}$ , on the other hand, will lead to a flat surface.

We have thus established a simple guideline which helps us to understand the influence of various regions in  $K$  space on the STM image. Another important point is the energy dependence. The higher the energy of a wave, the greater the effective range  $\lambda$  of its exponential

tail  $\exp(-\kappa z)$ , given by  $\lambda = 1/\kappa$ . For a step barrier this is seen in Eq. (1). A more realistic (imagelike) barrier shape will have an even greater increase of  $\lambda$  with energy, both because the classical turning point moves away from the surface and because the barrier immediately beyond the turning point is lower. Therefore the states highest in energy have the greatest chance of passing the tunneling barrier and will dominate the current. Consider the situation that the tip is higher in energy than the sample by a bias voltage  $V_B$ . The most important tip states are those at  $E_{F,\text{tip}}$ ; the most important sample states are unoccupied states at  $E_{F,\text{sample}} + eV_B$ . If we alter the voltage by  $\Delta V_B$ , the tip states will be essentially unchanged, but they will meet sample states at  $e(V_B + \Delta V_B)$  above  $E_F$ . The contrast in the  $I(V_B)$  spectrum is therefore likely

to reflect the electronic structure of the sample in this case. In general, the most important energies are  $E_F$  in the system higher in energy and  $E_F + V_B$  in the system lower in energy. States below these thresholds have less and less influence on the STM current. The spectral shape will thus reflect unoccupied states of the tip or of the sample, but it is unlikely to show much influence of the occupied electronic structure. This tendency has been seen experimentally, e.g., on Si(111).<sup>20</sup>

### B. Theoretical description of Ni(100)- $p(2 \times 2)$ C

The Bardeen formula, Eqs. (2) and (3), was formulated in terms of Green's functions:<sup>21</sup>

$$I(V_B) = \frac{2e^2}{\hbar\pi} \left( \frac{\hbar^2}{2m} \right)^2 \int dE \text{ trace} \left( (\overleftarrow{\nabla} - \overrightarrow{\nabla}) \text{Im}G_{\text{tip}} (\overleftarrow{\nabla} - \overrightarrow{\nabla}) \text{Im}G_{\text{sample}} \right). \quad (7)$$

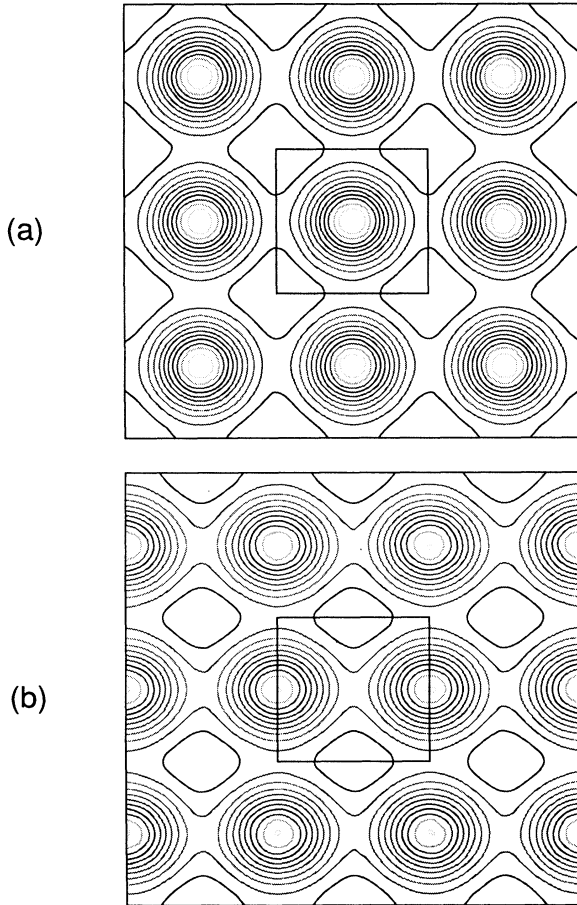


FIG. 5. Contour plot of the factor  $f(\mathbf{k}_{\parallel}, \mathbf{G}, \mathbf{g})$  which enters the STM current in the Bardeen approximation, as a function of  $\mathbf{k}_{\parallel}$ . A superposition for all vectors  $\mathbf{g}$  is shown. The parameters chosen are a step height  $V = 15$  eV, an energy  $E = 10$  eV, a tip distance  $z = 5$  Å, and a square lattice with a lattice constant  $a = 1.2$  Å. The square in the center is the first Brillouin zone. (a) The factor for  $\mathbf{G} = 0$ . (b) The factor for  $\mathbf{G} = (1, 0)$ .

The energy integration in Eq. (7) was performed for each bias voltage  $V_B$ , in contrast to an earlier calculation where a “single energy approximation” had been used.<sup>18</sup> The Green's function of the sample was calculated using a layer-KKR-based code. For the bulk, the non-spin-polarized potential from Moruzzi, Janak, and Williams<sup>22</sup> was used. The potentials of the surface layer were generated by overlapping atomic charge densities, adding an exchange-correlation energy using the Hartree-Fock-Slater  $X_{\alpha}$  scheme and tuning the exchange parameter to match the Nickel  $d$ -phase shift to that of the bulk. This approximate method has been successfully used before in investigations of the catalyst poisoning due to various adsorbates.<sup>1,5,6,8</sup> The surface barrier was described by a step potential with a work function of 5 eV. A single Ni atom from the bulk was used to represent the tip. The discrete bound states of the tip were broadened into “bands” by taking the energy complex inside the tip, with an imaginary part of 2 eV. This leads to a peak in the  $s$ -phase shift at 2 eV above the Fermi energy of the tip.

A model as simple as this cannot be expected to give quantitatively exact results. However, given the success of the similar calculations mentioned before, we expect to get at least the qualitative trend right. A similar approach was also used to describe the STM images of sulfur adsorbed on the Ni(100) surface, and the results were quite encouraging.<sup>18</sup>

For the clean Ni(100) surface, we used an unrelaxed geometry. The geometric arrangement of the C-covered surface was taken from a recent LEED measurement,<sup>23</sup> in which the coordinates of atoms down to the second Ni layer were determined. There it was found that the C atoms are located in fourfold hollow sites, only 0.12 Å above the first Ni layer. The first Ni layer is relaxed outwards by 11%, and the second Ni layer is buckled by 0.16 Å, with those Ni atoms directly underneath the C atoms being displaced outwards.

The STM image of the clean Ni(100) surface has been investigated before.<sup>18,24</sup> In the context of what was said earlier, one of the important points in the surface band structure is the presence or absence of band gaps. Bulk

Ni has a  $d$  band which is not completely filled, and an  $sp$  band which rises considerably above the Fermi energy. Therefore, in the energy range important for STM ( $E_F \pm 3$  eV), the (100) surface has occupied states near the  $\bar{\Gamma}$  point up to +3 eV, which gives a large noncorrugated part of the STM current. Consequently, the STM tip can rest at a relatively large distance. However, there are band gaps near the BZ boundary which can be understood from a projection of the bulk band structure in the [100] direction. For that reason, the corrugated part of the STM current is expected to be weak, resulting in a very flat surface. This is confirmed experimentally, with atomic resolution being achieved only at low voltages and at a large current ( $-15$  mV/2 nA),<sup>18,24</sup> i.e., when the tip is forced close to the sample.

The presence of C in the top Ni layer causes a dramatic change in the surface electronic structure around the Fermi energy. This is visible in the surface reflection coefficient  $R_{gg'}$ , which is the quantity central to our surface calculation. Its imaginary part enters, e.g., the local density of states. Viewing  $\text{Im}R_{00}$  as a function of both  $k_{\parallel}$  and  $E$  gives a representation of the surface band structure. There is now a surface band gap opening up at the  $\bar{\Gamma}$  point immediately above the Fermi energy, whose lower boundary in our calculation rises up to 1.8 eV at  $\bar{M}$  and somewhat less at  $\bar{X}$ . Within 2 eV below  $E_F$ , there is a complicated  $pd$ -hybridized structure and no band gap. Given the highly simplified model potential in our calculation, it is desirable to check these results against another calculated band structure. This is available (McConville *et al.*<sup>7</sup>), and it shows the same overall behavior: immediately below  $E_F$  down to  $-2$  eV, there is a dense structure of Ni  $d$ -C  $p$  states covering the whole BZ. Above  $E_F$ , however, there are few bands, mostly located in the bulk and presumably of Ni  $sp$  character. All this matches our results quite well, apart from a surface band in Ref. 7 which is of odd symmetry and rises from the  $\bar{\Gamma}$  point at  $E_F$  up to +2.4 eV at the point  $\bar{X}'$  [which is our  $\bar{M}$  because they use a simplified  $c(2 \times 2)$  geometry]. This band, which has its largest weight near the BZ boundary, does not show up in our calculation (i.e., there is no sharp maximum in  $\text{Im}R_{00}$  as usually associated with a surface state).

In search of the reason for this discrepancy, we first note that in Ref. 7, the  $p4g$  reconstruction of the surface was ignored. However, as mentioned in Ref. 7, experimental evidence suggests that the electronic structure is dominated by the  $c(2 \times 2)$  net and its associated symmetry. Rotating the Ni atoms straight in our calculation, we find considerable rearrangement of states below the Fermi energy but nearly no effect in the band gap above  $E_F$ . Therefore, the use of a simplified geometry in Ref. 7 cannot explain the surface state in question.

Another difference between the calculation in Ref. 7 and ours is the vertical position of the carbon atom. While the latest available structure data indicate  $d_{\perp} = 0.12$  Å,<sup>14</sup> McConville *et al.* (whose paper was published before Ref. 14) use  $d_{\perp} = 0.58$  Å. The sensitivity of this surface to the vertical position of the C atom has been noted before.<sup>3,4</sup> In fact hypothetically lifting the C atom to the same height as adsorbed sulfur or phospho-

rus makes carbon just as strong a poison as these. In order to check whether  $d_{\perp}$  was responsible for the difference between Ref. 7 and our calculation, we lifted the C atom to  $d_{\perp} = 0.6$  Å and repeated the calculation, with all other parameters unchanged. We found indeed that upon doing so, a strong surface state came up at  $\bar{M}$  at an energy of 1–1.5 eV. Lifting the C atom still further to  $d_{\perp} = 0.8$  Å caused the surface state to move up in energy to 2.5–3 eV. Therefore we believe that the reason for the surface band in Ref. 7 is at least partly the position of the C atom in this calculation.

The presence of the band gap above  $E_F$  gives rise to a highly unsymmetric voltage dependence of the STM data. We use the sign convention that electrons tunnel out of the sample, i.e., occupied states are probed, for  $V_B < 0$ , and electrons tunnel into the sample, probing unoccupied sample states, for  $V_B > 0$ . The calculated tip distance for various voltages is shown in Fig. 6. On the C-covered surface, the tip has to come closer than on the clean Ni(100) surface at all voltages, indicating an overall decrease of available states. This agrees with the reduction of the LDOS which was found previously in the vicinity of an adsorbed C atom.<sup>2,6</sup> The striking feature of Fig. 6, however, is the substantial asymmetry of the tip distance as a function of voltage. This reflects the presence of the gap at energies above  $E_F$ , which forces the tip to come much closer at positive voltages than at negative voltages.

As noted before, there is only little Ni influence in the surface electronic structure above and directly at the Fermi energy. Therefore it is not surprising that the  $p4g$  reconstruction, which consists of a displacement of the Ni

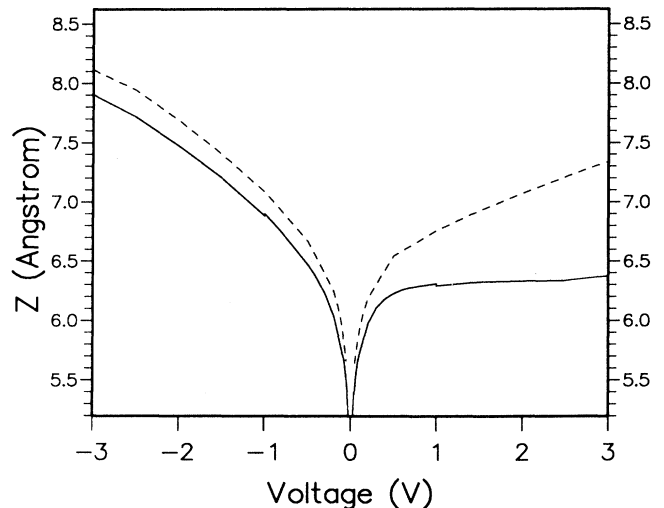


FIG. 6. The calculated tip-sample separation as a function of the bias voltage  $V_B$ , if the current is held constant at  $I = 1$  nA.  $V_B < 0$  means tunneling out of the sample, probing states below the Fermi energy,  $V_B > 0$  means tunneling into the sample, probing unoccupied states above the Fermi energy. Solid line, Ni(100)- $p(2 \times 2)$ C, dashed line, the clean Ni(100) surface.

atoms, does not show up in the calculated STM image (Fig. 7). In fact the Ni atoms are not seen at all. This is confirmed by the experimental image in Fig. 2. It could be argued that the  $p4g$  reconstruction involves higher-order Fourier coefficients which are strongly damped in the surface barrier, and that therefore this reconstruction cannot be seen in principle in a STM. However, on Ni(100)- $p(2 \times 2)N$  which has a very similar geometry and the same  $p4g$  symmetry,<sup>25</sup> the STM does see the reconstruction.<sup>26</sup> Thus its absence is nontrivial and strengthens our confidence in the approach presented here.

Since the tip is closer at positive voltage, and picks up mainly states from the Brillouin zone boundary, we expect the corrugation to be larger for positive voltage. The calculated corrugation as a function of voltage is shown in Fig. 8, and the expected trend is surely there: for negative voltages, the corrugation is at most of the order of 0.02 Å, while for positive voltages, it increases up to 0.1 Å. We would therefore expect the experiment to see some corrugation for  $V_B > 0$  but hardly any for  $V_B < 0$ . This turns out to be the case, as mentioned in Sec. II A: corrugation is observed at several positive voltages (+1 V, +1.5 V, and +2 V), but not at negative voltages. For very small negative voltages, Table I shows that the experiment does see corrugation there. In this case the tip is in very close proximity to the sample and the Bardeen approach Eq. (2) breaks down. The calculation in Fig. 8 was not performed for voltages smaller than 0.1 V. The result that the corrugation persists up to relatively high voltage is quite unusual for a metallic surface, because one would expect the tip to move away from the sample with increasing voltage, causing the higher-order Fourier coefficients to disappear. Our explanation for this is that the surface band gap forces the tip to stay close enough so that it gets all its current from states near the Brillouin zone boundary, which is the most important region in  $K$  space for corrugations

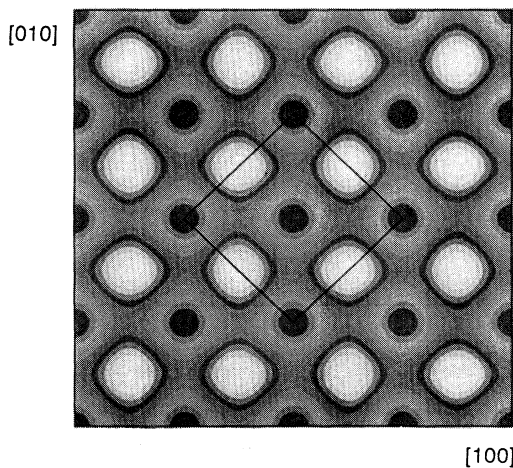


FIG. 7. Calculated STM constant current image of the Ni(100)- $p(2 \times 2)C$  surface for a current of 1 nA at  $V_B = +2$  V. Note that the rotation of the Ni atoms is not visible. The carbon atoms are mapped as depressions (dark spots). The unit cell is the same as in Fig. 1.

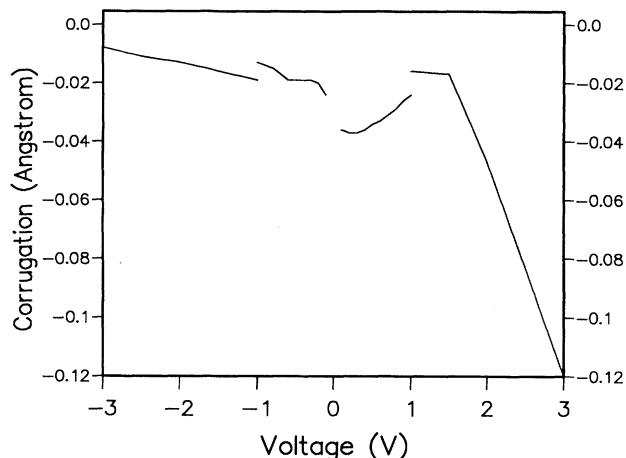


FIG. 8. The calculated corrugation as a function of the bias voltage, if the current is held constant at  $I = 1$  nA. Negative values mean that the carbon atoms are imaged as depressions. The jump at  $\pm 1$  V is a consequence of different energy mesh sizes in the integration. The mesh size was 0.1 eV between  $-1$  V and  $1$  V, and 0.5 eV elsewhere.

to appear.

Earlier theoretical studies of this surface found that a single adsorbed C atom acts as a repulsive electron scatterer which causes a decrease in the local DOS at the four nearest-neighbor Ni atoms, but not at those farther away.<sup>1,5,6,8</sup> It is therefore not surprising that the present calculation, using similar methods, leads to a calculated STM image in which the C atoms appear as depressions. This is at variance with the experimental result that C is imaged as a protrusion, albeit with a rather small height. It is difficult to pinpoint the precise reason for this discrepancy. Certainly, the potential of the sample is treated in a rather simplified way, but it ties in with the earlier results on the catalytic activity of this surface. Another possibility is that the tip structure played a role in the experiment. In order to clarify this, methods along the lines of, e.g., Sautet and Joachim<sup>27</sup> should be used which have been developed with quantitative crystallographic applications in mind. Our approach, however, is more qualitative, and designed to give information about big trends. In cases where the corrugation is large, this means that the sign of the corrugation is more reliable than its precise numerical value, which is difficult to obtain in any calculation due to a host of additional influences, such as elastic deformations of the tip, etc. In the present situation all we can do is state the discrepancy, which is made less severe by the fact that the experimental corrugation is very small and that the calculation does give a rather smooth surface.

The tip distance as a function of voltage, as shown in Fig. 6, is nearly constant above +1 V. This cannot really be true because it would imply constant current as a function of voltage, that is, zero differential conductivity (Fig. 9). One reason for this is the use of a step function for the surface barrier. As mentioned before, the

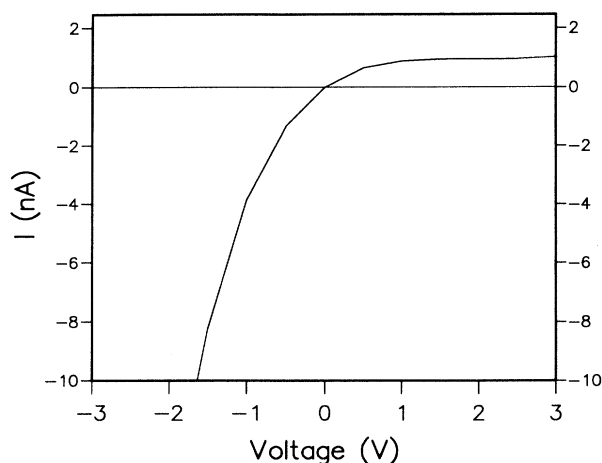


FIG. 9. The calculated current as a function of the bias voltage, at constant tip distance. The tip distance is fixed by demanding  $I = 1$  nA at  $V_B = +2$  V.

true barrier is of a different shape even for the surface in the absence of a tip. In going from the Fermi energy  $E_F$  to  $E_F + 3$  eV, the classical turning point moves outwards by 0.6–1 Å on various transition metal surfaces [Ni(100) (Ref. 28) and various Cu surfaces (Ref. 29)]. Also, the barrier height immediately after the turning point is lower than in a step. Thus we have a systematic trend in our calculation to underestimate the current, which becomes more pronounced for increasing voltage of either sign. The curve  $z(V_B)$  in Fig. 6 should increase more strongly than it does, for both signs of the voltage. The current as a function of voltage would then also increase more strongly, resulting in a curve which is unsymmetric about  $V_B = 0$  but not quite as unsymmetric as in Fig. 9. Experimentally, if we compare the current at +2 V with the one at -2 V, at various tip distances, we find that on average it is smaller by 0.71 (Table II). So there is some asymmetry in the experimental spectra which we interpret as indicative of the band gap in the sample. This is further corroborated by noting that the geometry of the tunneling junction—a sharp tip on one side and a flat surface on the other side—is sufficient to cause asymmetric  $I(V)$  spectra,<sup>30</sup> because of the enhanced electric field near the apex of the tip. This effect leads in general to *larger* currents at positive bias. The arguments given above can explain why this general tendency is reversed in our case.

#### IV. CONCLUSIONS

Experimentally, the Ni(100)- $p(2 \times 2)$ C surface has been found to be very smooth in the STM, with atomic resolution achievable only at positive voltage. However, corrugations could be observed for voltages as high as +2 V (electrons tunneling into the sample), which is quite unexpected for a metal surface. Neither the  $p4g$  reconstruction of the Ni atoms, although well established from other experiments, nor the Ni atoms themselves could be imaged in the STM. In order to explain these observations, we have invoked a simple model using muffin-tin potentials for the sample, a single muffin tin for the tip and Bardeen's approximation to calculate the tunneling current. The main result is that the Ni-C bonding gives rise to a surface band gap immediately above the Fermi energy, and that the Ni influence above and around the Fermi energy is rather small. The band gap causes the tip to come closer at positive voltages than at negative voltages, enabling it to pick up states from the Brillouin zone boundary that are more likely to produce corrugation. The gap extends up to 3 eV above the Fermi energy, which explains the occurrence of corrugations at higher voltages. These states are not very much influenced by the Ni atoms, so the reconstruction of the Ni is not visible through them. The calculation indicates an asymmetry of the  $I(V)$  spectrum: the conductivity at positive voltage should be less than at negative voltage. This is indeed observed, although less pronounced than in the calculation. The reason is presumably the approximate treatment of the barrier potential, which does not include the image tail and the enhanced electric field near the apex of the tip. Both effects would bring the calculated  $I(V)$  curve closer to the experiment. The calculated corrugation images the C atoms as depressions, whereas the experiment finds the C to be imaged as a protrusion. However, the experimental corrugation is quite small (around 0.02 Å for voltages above 0.1 V) and the calculation does give a rather smooth surface. This discrepancy indicates the limitations of the theoretical model used. Apart from this, however, our simple model is sufficient to explain most of the features observed on this surface.

#### ACKNOWLEDGMENTS

This work was supported by the United Kingdom Science and Engineering Research Council (SERC).

\*Also at Leverhulme Centre for Innovative Catalysis, Dept. of Chemistry, Liverpool University, Liverpool L69 3BX, UK.

†Also at Dept. of Chemistry, University of Manchester, Manchester M13 9PL, UK.

<sup>1</sup>R. W. Joyner, J. B. Pendry, D. K. Saldin, and S. R. Tennison, *Surf. Sci.* **138**, 84 (1984).

<sup>2</sup>J. M. MacLaren, J. B. Pendry, D. D. Vvedensky, and R. W.

Joyner, *Surf. Sci.* **162**, 322 (1985).

<sup>3</sup>J. M. MacLaren, J. B. Pendry, R. W. Joyner, and P. Meehan, *Appl. Catalysis* **25**, 9 (1986).

<sup>4</sup>J. M. MacLaren, J. B. Pendry, and R. W. Joyner, *Surf. Sci.* **165**, L80 (1986).

<sup>5</sup>R. W. Joyner, G. R. Darling, and J. B. Pendry, *Surf. Sci.* **205**, 513 (1988).

<sup>6</sup>G. R. Darling, J. B. Pendry, and R. W. Joyner, *Surf. Sci.*

- 221,69** (1989).
- <sup>7</sup>C. F. McConville, D. P. Woodruff, S. D. Kevan, M. Weinert, and J. W. Davenport, *Phys. Rev. B* **34**, 2199 (1986).
- <sup>8</sup>G. R. Darling, Ph.D. thesis, Imperial College, London, 1989.
- <sup>9</sup>P. J. Feibelman and D. R. Hamann, *Phys. Rev. Lett.* **52**, 61 (1984).
- <sup>10</sup>J. Tersoff and D. R. Hamann, *Phys. Rev. B* **31**, 805 (1985).
- <sup>11</sup>J. H. Onuferko, D. P. Woodruff, and B. W. Holland, *Surf. Sci.* **87**, 357 (1979).
- <sup>12</sup>K. H. Rieder and H. Wilsch, *Surf. Sci.* **131**, 245 (1983).
- <sup>13</sup>M. Bader, C. Ocal, B. Hillert, J. Haase, and A. M. Bradshaw, *Phys. Rev. B* **35**, 5900 (1987).
- <sup>14</sup>Y. Gauthier, R. Baudoing-Savois, K. Heinz, and H. Landskron, *Surf. Sci.* **251/252**, 493 (1991).
- <sup>15</sup>Th. Berghaus, A. Brodde, H. Neddermeyer, and St. Tosch, *Surf. Sci.* **193**, 235 (1988).
- <sup>16</sup>K. Takayanagi, Y. Tanishiro, S. Takahashi, and K. Yagi, *J. Vac. Sci. Technol.* **A 3**, 1502 (1985).
- <sup>17</sup>E. Kopatzki and R. J. Behm, *Surf. Sci.* **245**, 255 (1991).
- <sup>18</sup>A. Partridge, G. J. Tatlock, F. M. Leibsle, C. F. J. Flipse, G. Hörmandinger, and J. B. Pendry, *Phys. Rev. B* (to be published).
- <sup>19</sup>J. Tersoff, *Phys. Rev. B* **39**, 1052 (1989).
- <sup>20</sup>T. Klitsner, R. S. Becker, and J. S. Vickers, *Phys. Rev. B* **41**, 3837 (1990).
- <sup>21</sup>J. B. Pendry, A. B. Prêtre, and B. C. H. Krutzen, *J. Phys. Condens. Matter* **3**, 4313 (1991).
- <sup>22</sup>V. L. Moruzzi, J. F. Janak, and A. R. Williams, *Calculated Electronic Properties of Metals* (Pergamon, New York, 1978).
- <sup>23</sup>Y. Gauthier, R. Baudoing-Savois, K. Heinz, and H. Landskron, *Surf. Sci.* **251/252**, 493 (1991).
- <sup>24</sup>E. Kopatzki and R. J. Behm, *Surf. Sci.* **245**, 255 (1991).
- <sup>25</sup>L. Wenzel, D. Arvanitis, W. Daum, H. H. Rotermund, J. Stöhr, K. Baberschke, and H. Ibach, *Phys. Rev. B* **36**, 7689 (1987).
- <sup>26</sup>F. M. Leibsle, *Surf. Sci.* (to be published).
- <sup>27</sup>See, e.g., P. Sautet and C. Joachim, *Ultramicroscopy* **42**, 115 (1992); J. C. Dunphy, D. F. Ogletree, M. B. Salmeron, P. Sautet, M.-L. Bocquet, and C. Joachim, *ibid.* **42**, 490 (1992).
- <sup>28</sup>R. Schneider, K. Starke, K. Ertl, M. Donath, V. Dose, J. Braun, M. Grass, and G. Borstel, *J. Phys. Condens. Matter* **4**, 4293 (1992).
- <sup>29</sup>M. Grass, J. Braun, G. Borstel, R. Schneider, H. Dürr, Th. Fauster, and V. Dose, *J. Phys. Condens. Matter* **5**, 599 (1993).
- <sup>30</sup>A. A. Lucas, P. H. Cutler, T. E. Feuchtwang, T. T. Tsong, T. E. Sullivan, Y. Yuk, H. Nguyen, and P. J. Silverman, *J. Vac. Sci. Technol.* **A 6**, 461 (1988).

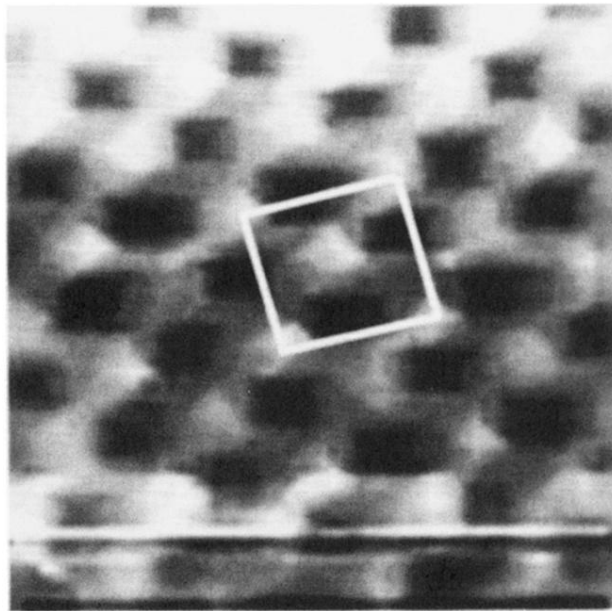


FIG. 2. A  $20 \text{ \AA} \times 20 \text{ \AA}$  image of the Ni(100)-(2 $\times$ 2)C  $p4g$  surface taken at  $-0.007 \text{ V}$ ,  $1.0 \text{ nA}$  with the  $c(2 \times 2)$  unit cell outlined.

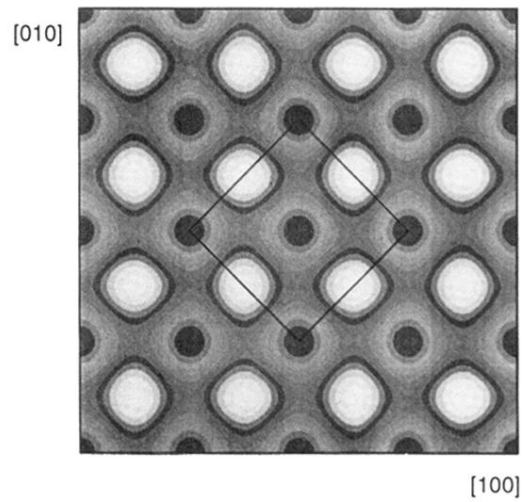


FIG. 7. Calculated STM constant current image of the Ni(100)- $p(2 \times 2)$ C surface for a current of 1 nA at  $V_B = +2$  V. Note that the rotation of the Ni atoms is not visible. The carbon atoms are mapped as depressions (dark spots). The unit cell is the same as in Fig.1.